Chemical Engineering Journal 218 (2013) 173–182

Contents lists available at SciVerse ScienceDirect

Chemical Engineering Journal

journal homepage: www.elsevier.com/locate/cej

Osmosis-assisted cleaning of organic-fouled seawater RO membranes

Guy Z. Ramon [1], The-Vinh Nguyen [2], Eric M.V. Hoek *

Department of Civil and Environmental Engineering, University of California, Los Angeles, CA, USA
California NanoSystems Institute, University of California, Los Angeles, CA, USA

HIGHLIGHTS

- Removal of Alginate with osmotic backwashing is comparable to chemical cleaning.
- Substantially higher cleaning efficiency achieved using a monovalent draw solution.
- Chemical 'loosening' of foulant layer is essential for backwashing effectiveness.
- Optimization of contact time, draw strength and chemical composition is required.

GRAPHICAL ABSTRACT

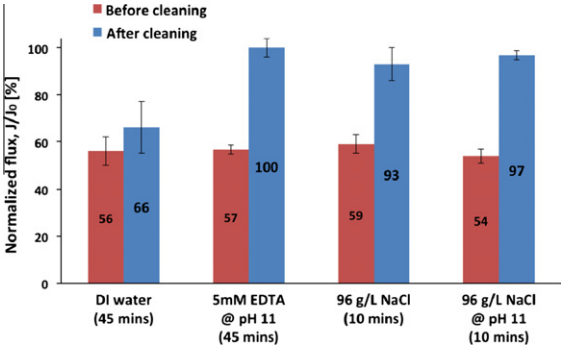

ARTICLE INFO

Article history:
Received 24 April 2012
Received in revised form 2 December 2012
Accepted 4 December 2012
Available online 8 December 2012

Keywords:
Reverse osmosis
Membrane fouling
Membrane cleaning
Osmotic backwashing
Direct osmosis
Desalination

ABSTRACT

Fouling of various kinds continues to limit membrane-based desalination and water treatment. Fouling is commonly countered through chemical cleaning of membrane elements, resulting in process downtime, membrane degradation and increased operation costs. Recent studies suggest that reversing permeate flux through RO membranes by dosing a slug of high salinity feedwater may offer an effective, chemical-free cleaning method. Herein, seawater RO membranes were fouled using alginic acid as a model seawater foulant and cleaned by osmotic backwashing with draw solutions of different salt concentration and chemistries. Flux recovery by osmotic backwashing was comparable with chemical cleaning (using caustic and a chelating agent); both recovered more flux than physical cleaning (rinsing with DI water). In particular, results illustrate the importance of combining chemical and physical mechanisms, the former contributing to 'loosening' of the foulant layer, and the latter facilitating its removal through fluid shear, enhanced by the presence of an osmotic backflow. Hence, osmotic backwashing may offer the potential for in-line, 'low-chemical' RO membrane cleaning, which would minimize discharge of cleaning chemicals to the environment and their impacts on RO membranes. Numerical simulations of the osmotic backwash cycle illustrate important time-scales and mass transfer limitations governing osmotic backwashing, through which operational insight may be obtained. The model offers a possible theoretical approach for optimization of RO membrane cleaning by osmotic backwashing.

1. Introduction

In reverse osmosis (RO) and nanofiltration (NF) membrane-based water purification systems, fouling of all kinds – colloidal deposition and organic adhesion, formation and growth of bacterial biofilms, and precipitation of sparingly soluble minerals – can limit plant performance, dominate operation and maintenance concerns and increase the cost of water produced. Even with

* Corresponding author at: Department of Civil and Environmental Engineering, University of California, Los Angeles, CA, USA. Tel.: +1 310 206 3735.
E-mail address: emvhoek@ucla.edu (E.M.V. Hoek).
[1] Present address: Department of Mechanical & Aerospace Engineering, Princeton University, Princeton, NJ, USA.
[2] Present address: Faculty of Environment, Vietnam National University-Hochiminh City, Hochiminh City, Viet Nam.

1385-8947/$ - see front matter © 2012 Elsevier B.V. All rights reserved.
http://dx.doi.org/10.1016/j.cej.2012.12.006

Nomenclature

B	membrane salt permeability (m/s)
c	concentration (mole/m^3)
D	molecular diffusion coefficient (m^2/s)
D^*	hindered diffusion coefficient, $\epsilon D/\tau$ (m^2/s)
h	half-channel height (m)
j	permeation rate (m^3/m^2 s)
L	channel length (m)
L_p	water permeability coefficient (m^3/m^2 s Pa)
ΔP	trans-membrane pressure (Pa)
Re	Reynolds number, 4h u_m/ν (–)
R_g	universal gas constant (J/mole K)
t	time (s)
T	temperature (K)
u	axial velocity component (m/s)
u_m	average axial velocity (m/s)
v	transverse velocity component (m/s)
x	axial coordinate (m)
y	transverse coordinate (m)
Y	scaled transverse coordinate, $2y/h$ (–)

Greek letters

α	ratio of pulse and bulk concentrations
β	osmotic coefficient, $2R_gT$ (J/mole)
ϵ	porosity (–)
ν	kinematic viscosity
τ	tortuosity (–)
τ_r	average hydraulic residence time, L/u_m
Π	osmotic pressure (Pa)

Subscripts

b	bulk
m	membrane
p	permeate

Abbreviations

CP	concentration polarization
MF	microfiltration
NF	nanofiltration
RO	reverse osmosis
UF	ultrafiltration

seemingly appropriate pretreatment processes in place, full-scale NF and RO system can suffer from biofouling and scaling, which increase applied pressure (i.e., energy and cost) and limit product water recovery, respectively. Hence, fouling control at real NF and RO plants has been a decades long battle despite exhaustive efforts to improve membrane and module properties, optimize pretreatment processes, and improve chemical cleaning agents.

In microfiltration (MF) and ultrafiltration (UF) membrane-based water treatment systems, particularly hollow fiber modules, periodically reversing the direction of filtration (a.k.a., hydraulic backwashing) has been successfully deployed at lab-scale and full-scale to combat short-term flux decline due to fouling (see, e.g., [1–3]). Historically, it was not possible to employ flux reversal via hydraulic backwashing for NF and RO membranes due to their composite structure; the pressure differential required and perhaps the hydraulic drag created could lead to mechanical failure by composite de-lamination. It is therefore common practice for RO/NF plants to produce water in a forward filtration mode for months at a time while employing periodic chemical cleaning, as needed, due to buildup of excessive trans-membrane or trans-module pressure drops. Both in situ (a.k.a., clean-in-place or CIP) and ex situ cleaning of NF/RO membrane modules are employed in practice. In either case, the standard approach is that the portion of the plant being cleaned is taken off-line [4]. This results in significant process downtime. Moreover, since cleanings are employed over relatively large time intervals (3–12 months apart) they may not completely remove fouling materials accumulated within a membrane module.

Recent studies provide some indication that reversing the direction of filtration for NF and RO membranes via direct osmosis (a.k.a., osmotic backwashing) may offer a fouling mitigation method analogous to hydraulic backwashing in MF and UF systems [5–8]. However, prior studies of osmotic backwashing are fairly empirical in nature, based on pilot-scale or full-scale installations. While the empirical evidence that osmotic backwashing can be an effective means of controlling short-term flux decline is compelling, very little is known about osmotic backwashing removal efficiency for different types of fouling materials; even less is known about the fundamental mechanisms governing these processes.

Osmotic backwashing may be induced when the feed-side osmotic pressure exceeds the applied hydraulic pressure across the membrane. This may be accomplished in several ways: reducing the feed-side applied pressure, raising the permeate pressure, or injecting the feed channel with a pulse of a high-concentration solution (osmotic draw solution). However, hydraulic pressure equilibration will induce substantial osmosis only if the feed stream is sufficiently concentrated, e.g., in the case of seawater; the injection of a high-concentration pulse allows this method to also be used for low-salinity feeds such as brackish- or wastewater. The idea of osmotic backwashing is not a new one, and dates back 30 years [9]. Patents have been issued, which elaborate on technical ways by which to incorporate an osmotic backwash into large-scale RO system design (see, for example, [10]) and the idea is slowly permeating the industry. Theoretical models have been used to explore the characteristics of the transient osmotic flow during a backwash cycle [11–13]. These have been shown to be useful in elucidating the relative importance of the various transport mechanisms present at different time-scales and illustrating the possible magnitude of osmotic fluxes achievable.

For any practical scenario, the process becomes far more complicated due to the presence of a complex, multi-component fouling layer accumulated at the membrane surface. When considering the possible removal of such accumulated foulants through flux reversal (as in a backwash cycle), does one treat this process as a purely physical one? In that case, the sole mechanism for removing material deposited at the membrane surface is a vertical drag force exerted by the reversed permeation through the deposited layer. This may indeed be the case when the time scales for deposition and release are short, i.e., as with rapid hydraulic back-pulsing [1], but seems somewhat naive when considering longer time-scales between each backwash cycle, which are more practical for an osmosis-induced backwash process. In such cases, some consideration of physical–chemical interactions within the deposited layer and with the membrane must be included. Some evidence of such effects has been recently reported on the effect of ionic composition on backwash efficacy in UF, suggesting that when charge screening effects are important, employing de-mineralized water for the backwash cycles resulted in increased efficiency [14,15].

In this spirit, we hypothesize that osmotic backwashing may have varying efficiencies when tackling different fouling types, e.g., colloidal deposition, organics, mineral scaling or biofouling,

each with its specific physical–chemical characteristics and interactions with the membrane surface and within the fouling layer. Such variability may reflect on the backwash frequency necessary for fouling reversal, backwash duration and magnitude as well as possible coupling with chemical additives in the osmotic draw solution. Therefore, an osmotic backwash employed in a wastewater reclamation plant may require a different approach to that employed in a seawater desalination plant due to the variation in both feed and membrane characteristics.

This type of approach is complementary to what may be viewed as an emerging paradigm in membrane cleaning: specific chemical targeting of characteristic foulants present in the feed stream, matched with an appropriate cleaning agent [16–23]. Such an approach offers the potential advantage of increased cleaning efficiency, which may translate into shorter cleaning times and, hence, less operational downtime and reduced membrane degradation; the latter effect may possibly be reduced further by not exposing the membrane to unnecessary harsh chemicals. Advanced cleaning strategies require an intricate, mechanistic understanding of the physical–chemical interactions governing membrane fouling. Both membrane–foulant and foulant–foulant interactions must be taken into account for a targeted cleaning solution and procedure to be truly effective. Evidence of this is slowly accumulating in the literature. Notably, understanding of adhesion forces and specific ion-interactions of model organic foulants has produced efficient cleaning strategies based on targeting these vary same interactions; disrupting or otherwise weakening them enables their subsequent removal from the membrane surface via physical means. Specifically, the ionic composition of the feed, e.g., the presence of divalent cations, has been shown to strongly correlate with fouling severity for organic colloids such as Alginic acid and natural organic matter [16–18]. In the absence of divalent cations and under otherwise identical operating conditions, the observed fouling severity was substantially lower [19]. The enhanced fouling in the presence of divalent cations has been associated with cross-linking (calcium bridging) creating stable complexes, which are more difficult to remove. Weakening these complexes using metal chelating agents such as EDTA [17,19] and possibly even simple ion exchange with a NaCl solution [18] has been shown to facilitate surprisingly effective cleaning and significant flux recovery. Moreover, it has been suggested that synergistic effects may exist between the chosen cleaning solution and its interaction with the targeted foulant; an example of this is the cleaning of organic-fouled RO membranes using the combination of a chelating agent (or a monovalent salt) at an elevated pH of 11. Finally, a recent study has shown that when various foulants are present, which is certainly a realistic scenario, a properly selected dual-stage cleaning procedure may yield nearly complete flux recovery [23].

These results all suggest that where the underlying fouling mechanisms are well understood, a tailored cleaning solution may be found for which an optimal efficiency is achieved. In this paper an attempt is made, for the first time, to systematically examine the cleaning efficiency achieved using cleaning protocols assisted by the presence of an osmotic backwash.

2. Model formulation

Essentially, the model solves the transient convection–diffusion equation in the membrane feed channel, coupled with a convection–diffusion equation that describes the concentration field in the support-side of the membrane. The equations are coupled through expressions that relate the water flux and salt flux to the concentrations on either side of the membrane, i.e., in the feed and permeate domains. The computational domain used in the simulations is a parallel-plate geometry, as depicted schematically in Fig. 1. It is bounded by upper and lower membrane walls, as well as the feed inlet/outlet boundaries. Owing to symmetry, only the bottom half of the channel is considered, thereby reducing the computational requirements. The model is two-dimensional, assuming that the third dimension (the channel width) is sufficiently large.

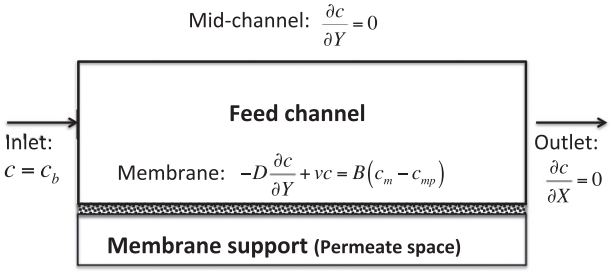

Fig. 1. Schematic drawing of the model domain and boundary conditions used.

While the basic features of the model employed in this study are similar to those presented previously in [12], the configuration studied, time-scales involved and ultimate use of the model are different. Specifically, the previous study was focused on the initial dissipation of a concentration–polarization boundary layer upon the elimination of the hydraulic pressure. The short time dynamics of this process were studied, addressing the relative importance of diffusion and advective processes in the axial and transverse direction. A main assumption in the previous simulations was that the membrane is fully retentive, since it was shown that leakage through the membrane is of small impact at short times. In the present study, focus is on backwashing induced by a concentrated draw solution, presenting a higher driving force for solute transport through the membrane; thus, salt leakage is expected to be more significant. In addition, longer durations are simulated, since it was experimentally observed that flux continued to decline over longer time scales. The simulations were then used to assess whether the idea of internal concentration polarization, incorporated more rigorously into the model and simulations, would provide a mechanistic understanding of the experimentally observed trends.

2.1. Model equations

2.1.1. The feed channel

In the feed channel, a solute mass balance provides the following 2D convection–diffusion equation:

$$\frac{\partial c}{\partial t}+u\frac{\partial c}{\partial x}+v\frac{\partial c}{\partial y}=D\left(\frac{\partial^2 c}{\partial x^2}+\frac{\partial^2 c}{\partial y^2}\right), \tag{1}$$

where $c(x,y,t)$ is the solute concentration, D is the solute molecular diffusion coefficient, x, y denote the axial and transverse coordinates, respectively, t is the time and u, v are the axial and transverse velocity components, respectively.

2.1.2. The permeate space

In the permeate space, the mass transfer process is approximated as one-dimensional; this is justified by the fact that the transverse velocity component (the permeation rate) is expected to dominate the velocity field within the porous membrane support structure. A realistic depiction of the permeate side in a commercial spiral-wound RO module requires a three-dimensional model, since the permeate is distributed through a central collection tube and flows outward in a direction that is generally perpendicular to the feed flow. Therefore, the 1D assumption results in

significant reduction of computational resources. It is anticipated that the general trends of permeation should be well-captured by an averaged permeate concentration field along the membrane, certainly for the experimental system employed herein.

During an osmotic backwash cycle, salt accumulates on the permeate side of the membrane, primarily within the support structure of the composite membrane; this causes a particularly severe case of internal concentration polarization (CP), well known in related studies on forward osmosis (FO) [24]. The porous support of the membrane provides a low-porosity, tortuous media that results in the hindered diffusivity of osmotic draw salts being less than 5% of their bulk fluid diffusivity. Internal CP is more severe during osmotic backwashing, compared with FO operation, since there is no crossflow on the permeate side; therefore, transport away from the membrane is driven solely by diffusion.

With these assumptions, the convection–diffusion equation on the support side of the membrane is:

$$\frac{\partial c_p}{\partial t} + v\frac{\partial c_p}{\partial y} = D^*\frac{\partial^2 c_p}{\partial y^2}, \tag{2}$$

where c_p denotes the concentration in the permeate space and D^* is a 'hindered' diffusion coefficient (a common assumption is that it is related to the 'free' liquid diffusivity via $D^* \sim \epsilon/\tau D$, in which ϵ, τ are the porous medium porosity and tortuosity, respectively).

2.1.3. The velocity field

In principle, the velocity components u and v are unknown and are found through a solution of the Navier–Stokes equations, coupled with the mass balance Eqs. (1) and (2). As found in a previous study [12], a significant computational simplification (with minor accuracy loss) may be made by assuming a fully developed, laminar, velocity profile, in which the axial velocity component is

$$u(Y) = 6u_m Y(1-Y), \tag{3}$$

where u_m is the average cross-flow velocity and $Y = 2y/h$ is the scaled transverse coordinate, with h denoting half the channel height.

The transverse component of the velocity is the permeation rate, which we express using a linear osmotic pressure model, as follows:

$$-v = j_w = L_p(\Delta P - \beta\Delta c), \tag{4}$$

in which L_p denotes the membrane water permeability, ΔP is the trans-membrane pressure drop, $\beta = 2R_gT$, where R_g is the universal gas constant, and T is the absolute temperature. $\Delta c = c_m - c_{mp}$ is the concentration difference across the membrane with c_m, c_{mp}, denoting the membrane surface concentrations at the feed and permeate sides, respectively. We also note that the feed-side membrane concentration used as a variable in the 1D permeate space (for determining both the solute and water flux expressions) is a channel-averaged value.

2.2. Boundary conditions

At the feed channel inlet, a 'pulse' of constant concentration is specified as

$$c(x=0,y,t) = c_b(1 + \alpha F[t,t_i,t_o]), \tag{5}$$

where $F = (1+e^{-20(t-t_i)})^{-1} - (1+e^{-20(t-t_o)})^{-1}$ is a function which rapidly varies between 0 and 1, creating a rectangular pulse defined by the time of initiation, t_i, and the time of termination, t_o; the interval $t_i - t_o$ determines the duration of the pulse. The constant α controls the concentration of the pulse relative to that of the bulk.

At the outlet, it is assumed that advection dominates over diffusion, hence

$$\frac{\partial c}{\partial x} = 0, \quad x = L. \tag{6}$$

A symmetry condition is specified at the mid-channel plane,

$$\frac{\partial c}{\partial y} = 0, \quad y = h. \tag{7}$$

The solute flux balance at the membrane surface is

$$-D\frac{\partial c}{\partial y} + vc = B(c - c_{mp}), \quad y = 0, \tag{8}$$

where B is the membrane salt permeability. This condition is also used in the support side of the membrane, where the membrane surface concentration from the feed side is integrated (reducing the axial dependence into a single value to be implemented in the 1D equation describing mass transfer in the support).

Finally, an additional boundary condition is required in the support side; a useful approximation is a 'boundary layer' type assumption, whence the concentration gradient decays far from the boundary, viz.

$$\frac{\partial c_p}{\partial y} = 0, \quad y \to -\infty, \tag{9}$$

taken here in the negative direction since the origin of the y-axis is the membrane surface, pointing positively outward into the feed channel. The permeate domain length was chosen such that this assumption was always satisfied and calculations proved to be insensitive to this condition, under the conditions employed in this study. In fact, the performed calculations indicated that the region over which concentration polarization developed within the permeate space was on the order of 50 μm thick, substantially less than the thickness of the support structure of commercial RO membranes, which is approximately 150 μm, including the non-woven PET layer.

2.3. Computational details

The model equations were solved using a commercial finite-element package (Comsol Multiphysics v3.5a). The feed and permeate domains were meshed using a structured, boundary-layer type mesh with rectangular elements, with an exponential variation in mesh density decreasing from the membrane surface outward; this enabled a significantly more efficient computation while retaining accuracy where the largest concentration variations were expected in the system. Mesh refinement was carried out to ensure the independence of the solution on the mesh.

3. Experimental

3.1. Feed and draw solutions

The feed stream for all fouling experiments contained a commercial sea salt (Instant Ocean; Spectrum Brands, Inc., Atlanta, Georgia) at a fixed concentration of 32 g/L. Draw solutions used were either the feed stream itself, a 64 g/L sea-salt solution simulating RO brine, and NaCl solutions (ACS reagent grade, Fisher Scientific, Pittsburgh, Pennsylvania) at concentrations of 32, 64 and 96 g/L. Simulated seawater solutions were prepared by dissolving 32 g/L of Instant Ocean in deionized water under stirring conditions, and subsequent filtration through a 0.45 μm membrane (Regenerated Cellulose, Whatman), using a glass vacuum filtration device; this step was made to ensure that no particulates would be present in the re-constituted seawater feed. The organic foulant used in this study was Alginic acid from brown algae, which is a commonly used surrogate for organic molecules found in seawater (sodium alginate; Sigma–Aldrich, St. Louis, Missouri). For each

experiment, 2 g/L stock solutions were prepared by dissolving 1 g of dry alginate powder (as received) in 500 mL of deionized water under vigorous stirring.

3.2. Seawater RO test apparatus

All seawater RO fouling experiments were conducted using a custom fabricated bench-scale cross flow RO desalination simulator (for details, see supporting material, Fig. S1). The system contains six plate-and-frame membrane modules with individual membrane area of 19 cm^2 (7.6 cm long by 2.5 cm wide) and a channel height of 2 mm. The six modules are fed a common pressurized feed solution. The commercial seawater RO membrane used in this study was SW30HR-LE (Dow Water Solutions, Edina, Minnesota, USA). The experimentally measured water and salt permeabilities were $4 \pm 0.5 \times 10^{-12}$ ($ms^{-1}\,Pa^{-1}$) and $3 \pm 1 \times 10^{-8}$ (ms^{-1}), respectively. The feed concentration was kept constant by re-circulating both concentrate and permeate into the feed tank. A cylindrical, 10 L feed tank was used, stirred with a magnetic stirrer. Feed water temperature was maintained at 25 ± 0.1 °C by a laboratory recirculating heater/chiller (NTE RTE7; Fisher Scientific, Pittsburgh, Pennsylvania, USA). The feed water was pressurized and fed through the RO modules by a diaphragm pump (Hydracell; Wanner Engineering, Minneapolis, Minnesota, USA). During fouling tests, the applied pressure was kept constant and flux decline monitored by a digital flowmeter (Optiflow 1000; Agilent Technology, Foster City, California, USA). Feed and permeate conductivities were monitored at the beginning, end, and periodically throughout the fouling experiments (Accumet XL20, Cole Parmer, Barrington, IL).

3.3. Fouling and cleaning experiments

Each fouling and cleaning experiment followed the same protocol, which began with de-ionized water filtration at 58.6 bar (850 psi) to account for compaction and other sources of flux decline inherent to bench scale crossflow membrane filtration systems. Fresh membrane coupons were used at the start of each experiment. The flow in the channel was laminar, with an average flowrate through each cell maintained at 0.1 L/min, corresponding with a Reynolds number of ~400 (an average velocity of 10 cm/s). During backwashing cycles, purging the applied pressure resulted in an increase of the flowrate, increasing the Reynolds number to ~500. Next, the pure water permeability of the membrane was determined by varying the pressure and measuring the permeate flux through each membrane. This was followed by filtration of a foulant-free seawater electrolyte (32 g/L Instant Ocean dissolved in DI water) at an applied pressure of 55 bar (800 psi), during which both permeate flux and rejection were monitored for the un-fouled, compacted membranes. Next, the designated osmotic draw solution was circulated with no pressure applied to establish the un-fouled, compacted membrane forward osmosis permeation rate. The forward osmosis permeation rate was determined from the measured decrease in mass of a vial containing de-ionized water (placed on a digital scale) with the permeate flow tubing immersed in the vial.

Following the conditioning steps described above, a pre-dissolved alginate solution was added to the feed tank to achieve a feed concentration of 100 mg/L. Accelerated fouling tests were run for 5 h, after which various cleaning procedures were evaluated. The cleaning procedures applied were either: (1) physical cleaning, which involved recirculating de-ionized water for 45 min with no permeation; (2) chemical cleaning, during which the membrane was flushed with a solution of 5 mM di-sodium-ethylene diamine tetra-acetate (EDTA) at a pH of 11 adjusted by addition of NaOH (ACS Grade NaOH, Fisher Scientific); or (3) osmotic cleaning, which consisted of recirculating a high salinity feed solution for 10 min followed by physical cleaning as described above in procedure 1. Draw solutions used in the osmotic cleaning experiments were either seawater mixtures at 32 and 64 g/L (simulating seawater and seawater RO brine, respectively) or NaCl solutions with a concentration of 32, 64 and 96 g/L. During a cleaning cycle, the back pressure regulator was completely opened, so there was no permeation under such conditions. Once the cleaning was completed, flux recovery was determined by restoring the applied pressure and measuring the flux of the seawater feed.

The cleaning protocols were based on the following considerations. The chemical cleaning protocol was based on a recipe shown in previous studies to be effective in removing organic fouling (e.g., [19,22,23]), and a 45 min rinse was based on the time necessary to achieve complete flux recovery. For consistency, the same time was then employed for the DI water rinse (physical cleaning). Backwash duration was selected based on model calculations of draw solution pulse propagation, and experimental observation of the flux decline during a backwash cycle. A 10 min backwash time was chosen since it corresponds with very long pulses (as discussed below in Section 4.1.1); in addition, since it was observed that backwash permeation continuously declined, the chosen duration still allowed some permeation to be retained (at approximately 30–40% of the initial flux, depending on the draw strength). The choice of draw solutions was made based on the notion that in a SWRO plant, the natural availability of brine presents an opportunity to use it as the draw solution for the osmotic backwash. However, the literature suggests that divalent cations (in particular, Ca^{2+}) complex with organics and seawater RO membranes (see, e.g. [18]). Since divalent cations would be at very high concentrations in seawater RO brine it would not be expected to remove complexed organics from seawater RO membranes; however, a divalent free salt solution could exchange Na^+ ions for Ca^{2+} ions, thereby reducing complexation and helping remove adsorbed organics. A concentration range for NaCl was selected to probe the effect of the draw solution osmotic pressure (driving force of the permeation) on reverse permeation rate and cleaning efficacy.

4. Results and discussion

4.1. Simulation results

In the following section, results obtained from numerical simulations are presented, with two goals in mind. First, insight gained from the simulated dynamics of the process motivated choices made with respect to experimental conditions. Second, these illustrative results extend our understanding of the process dynamics at long times, which appear to be important time scales not previously investigated (e.g., in [11–13]).

4.1.1. The propagation of a concentration pulse

When considering an osmotic backwash cycle induced by a pulse of high concentration draw solution, several parameters emerge which may play a key role in the effectiveness of the process. It has previously been shown that a backwash cycle is controlled by different transport mechanisms at different time-scales [12]. In general, the combined effects of osmotic draw strength and convective mass transfer conditions in the feed channel control the osmosis-induced flow through the extent of dilutive concentration polarization on the membrane feed side.

For a full-scale system, dilution along the membrane elements must also be considered; such dilution will reduce the osmotic driving force, eventually reaching a point where flow reversal no longer occurs. Longitudinal dispersion (Taylor dispersion) also

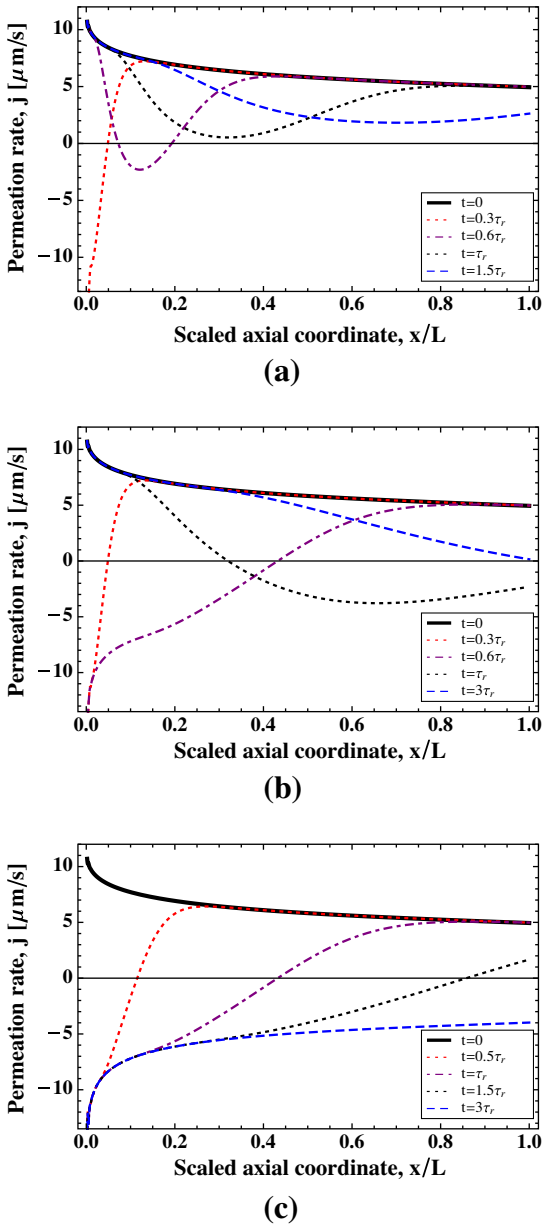

Fig. 2. The transient propagation of a high concentration pulse through the channel. Shown here is the axial distribution of the permeation rate at different times, represented as fractions of the average hydraulic residence time, $\tau_r = L/u_m$. (a) A 'short' pulse with an injection time of $0.2\tau_r$. (b) Pulse injection time τ_r. (c) Pulse injection time of $5\tau_r$. Calculations are made with $L_p = 3.5 \times 10^{-12}$ m/(s Pa), $B = 3 \times 10^{-8}$ m/s, $c_b = 2.5$ M, $Re = 200$ and $\Delta p = 60$ bar.

results in a dilutive effect, which ultimately scales with the channel length. However, the latter effect will become important only if the characteristic time of the pulse is shorter than the average hydraulic residence time of the channel. it is useful to define this characteristic convective time scale, $\tau_r = L/u_m$, the average hydraulic residence time, to illustrate the dynamics of a propagating pulse. The pulse dilution as it traverses the length of the channel is simulated for relatively short or long pulses, taken here as having a duration equal to $\sim 0.2\tau_r$ (Fig. 2a), $\sim\tau_r$ (Fig. 2b) and $\sim 5\tau_r$ (Fig. 2c). The dilutive effect is clearly observable in Fig. 2, which shows the flux distribution along a membrane channel at different times, scaled in terms of the hydraulic residence time, τ_r. Note that the pulses are of equal draw strength (2.5 M or ~16% by weight), producing the same initial osmotic permeation, and evolve from the same initial condition representing steady-state RO operation at an applied pressure $\Delta P = 60$ bar; this applied pressure is unchanged during the introduction of the pulse into the feed channel.

The calculated examples are illustrative of the dilution effect and its potential impact on the effectiveness of the backwash; when the pulse duration is chosen to be equal to the characteristic convective time scale (hydraulic residence time), it successfully reversed the permeation along the full length of the membrane channel (see Fig. 2b); however, the permeation rate is all but lost by the time the pulse reaches the end of the channel, at a time equal to $3\tau_r$. Conversely, for a shorter pulse, here chosen to be 20% of the characteristic residence time, the pulse loses its effectiveness after 30% of the channel (see Fig. 2a). Finally, for the longest pulse duration ($5\tau_r$, see Fig. 2c), the pulse propagates to the point where a steady axial distribution is reached (still locally transient); under such conditions, the maximum achievable osmotic permeation affects the channel throughout its length.

This dilutive effect, which dictates that the backwash strength will decline with channel length, is unavoidable; however, as these simulations illustrate, allowing sufficient time for the pulse to affect the full length of the channel to its maximum capacity is possible. Specifically, this would have important implications for long membrane trains, which may be up to 8 m in length. For example, in an 8-element spiral-wound module operating with a linear velocity of ~0.1 m/s (Reynolds number of ~200), this characteristic time would be 80 s. A shorter pulse would necessitate a higher concentration so as to maintain flow reversal throughout the system. This obviously calls for optimization to be done; however, the point to consider is that there may be a lower boundary on how short a pulse may be while still ensuring effectiveness. Ultimately, the determining factor may be the duration of the backwash rather than its intensity, in which case the pulse may be inherently longer than the system characteristic time-scale. This theoretical observation was used as a guide in choosing our experimental backwash duration, which we took to be extremely long in terms of the channel hydraulic residence time (approaching infinity in the mathematical sense).

4.1.2. Concentration polarization during a long pulse

The previously shown simulations indicate that a relatively long pulse duration is required for a fully effective backwash cycle; it is therefore insightful to consider the time-evolution to the osmotic permeation rate over longer time periods. Specifically, we look at conditions which mimic our experimental system – a 10 min cycle, the draw concentrations and range of crossflow velocities (in terms of the channel Reynolds number), as well as membrane water and salt permeabilities. Unlike the results shown in the previous section, here the applied pressure was set to zero at the onset of a backwash cycle, as in our experimental protocol.

Figs. 3a/b show the transient permeation rate (channel-averaged and scaled against the initial permeation rate) during an osmotic backwash cycle, when either the crossflow velocity or draw concentration were varied. These figures clearly illustrate the two time scales involved in the process. At short times, dilution (which diminishes the osmotic driving force) is dominated by the transverse convective transport induced by the osmotic permeation; this dilution is rapid and, for a fully retentive membrane, should result in a steady-state permeation rate dictated by the mass transfer produced by crossflow-induced convection in the feed channel. Steady-state operation is also reached in FO systems since axial convection is present on both sides of the membrane. In the case of an osmotic backwash, however, such a steady-state is never reached, due to the poor mixing conditions which exist in the permeate space. Salt is transported through the membrane, driven by the high concentration difference, and accumulates in the permeate space. As a result, the osmotic flux will continuously decline, albeit at a slow rate, until the concentration on either side

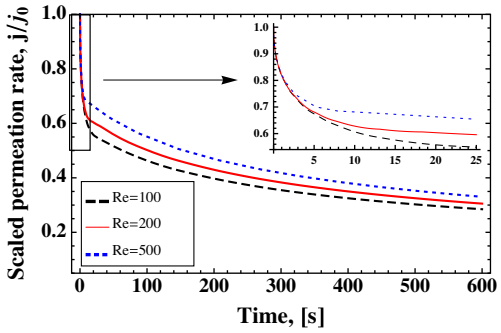

(a)

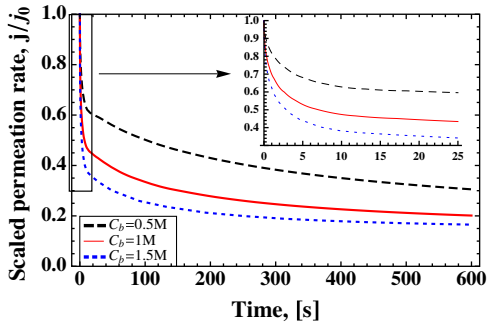

(b)

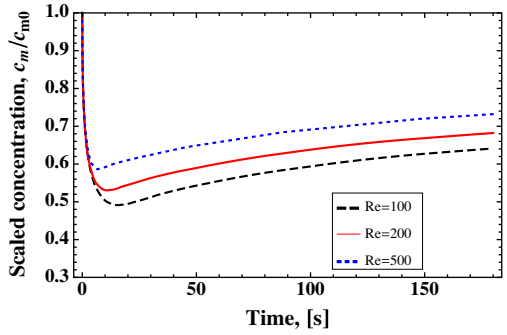

Fig. 3. Simulation results, illustrating backwash dynamics: (a) Scaled flux decline over time, for different Reynolds numbers, representative of external convection; the inset shows the short time decline corresponding with external concentration polarization (b) Same as (a), for different draw solution concentrations, at $Re = 200$. (c) The time evolution of the channel averaged, membrane surface concentration. Unless otherwise noted, calculations are made with $L_p = 3.5 \times 10^{-12}$ m/(s Pa), $B = 3 \times 10^{-8}$ m/s, $c_b = 1$ M and $Re = 500$.

of the membrane is equilibrated and no driving force exists. As may be seen in Figs. 3a/b, our numerical simulations suggest that the time scale for this process is on the order of several minutes, while the short-time external dilution occurs on the order of 10–20 s or less, depending on the crossflow rate (or, more generally, the Reynolds number). Further, it may be seen that when the draw solution concentration is varied, the general trend of the flux decline curves remains identical. This is in contrast with the calculations where the crossflow velocity is varied, in which case the transition between the initial decline, governed by external CP, and the slow decline caused by internal CP, occurs faster as the crossflow velocity (Reynolds number) is increased. A similar trend is observed in Fig. 3c, which shows the evolution of the channel-averaged membrane surface concentration; an amusing feature seen here is the increase in surface concentration which follows the rapid dilution. This may be understood by considering that the surface concentration changes primarily due to the presence

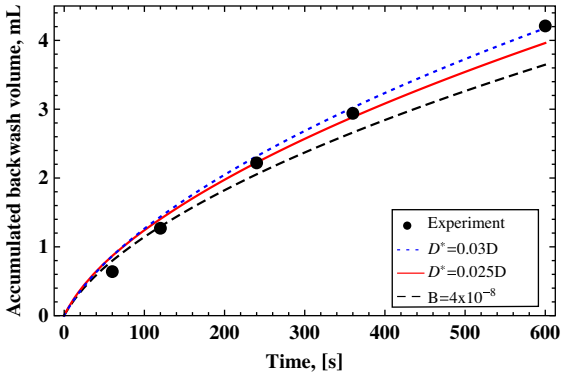

Fig. 4. Accumulated permeate volume – model predictions vs. experimental measurements, illustrating model sensitivity to parameters controlling the severity of internal concentration polarization. Unless otherwise noted, calculations are made with $L_p = 3.5 \times 10^{-12}$ m/(s Pa), $B = 3 \times 10^{-8}$ m/s, $c_b = 1$ M and $Re = 500$.

of the osmotic permeation; thus, as the permeation rate declines, so does the degree of polarization.

Finally, we briefly compare some representative model predictions with experimental measurements of the accumulated permeate volume during a 10-min osmotic backwash cycle. Fig. 4 shows calculations made for the case of a 1 M draw solution, with parameters corresponding with the experimental conditions. The calculated trend seems to follow the experimental value quite well. However, it should be noted that this calculation is not fully predictive, since we have no information on the transport in the support side, which dominates flux decline during most of the cycle. This information is essentially 'lumped' within the hindered diffusivity, D^*, which is unknown. Based on some information from the FO literature, where the related 'structural parameter' has been evaluated for commercial RO membranes (see, e.g., Yip et al. [25]), we estimate the hindered diffusivity to be on the order of ~2–3% of the molecular diffusivity. The calculations shown here illustrate the sensitivity of the model to slight variations of this parameter, as well as slight changes to the salt diffusivity; these are the main parameters which control the severity of internal CP.

4.2. Experimental results

4.2.1. Osmotic permeation of clean and fouled membranes

Fig. 5 shows the permeation rate, averaged over the full 10 min of the backwash, for draw solutions comprised of either NaCl at concentrations ranging between 32–96 g/L or 32/64 g/L Instant Ocean (the raw data of accumulated volume vs. time is available in the supplementary material). As may be seen, the experimentally measured osmotic permeation rates generally followed an expected trend of increasing with higher draw concentration. It is important to note, however, that these results should not be held strictly against any simple theory. This is mainly due to the fact that a 10-min average is not predictable solely based on draw concentration. Specifically, since no information is known regarding the transport on the support side, which governs a large portion of the accumulated volume, no conclusions may be made in a strictly quantitative base. Moreover, there may be unknown variabilities in the support structure between different membrane coupons used in the experiments.

Fouled membranes exhibit a reduced osmotic-permeation rate, which is also expected since the fouling layer reduces the overall permeability of the system. It is interesting, however, to note the noticeably reduced permeation rate measured for the fouled membranes, even when higher draw solutions were used. In general, this means that the effective driving force is substantially

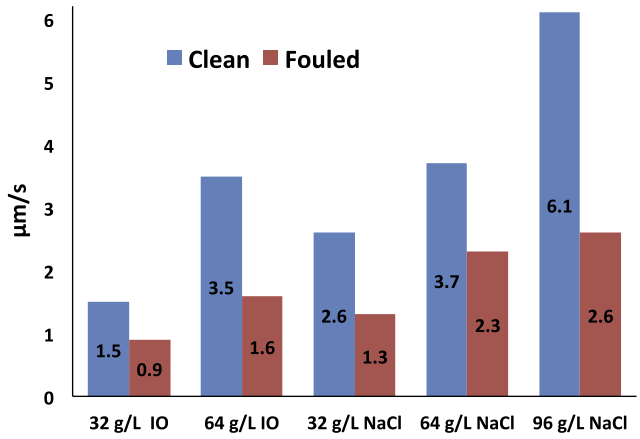

Fig. 5. Osmotic permeation rates (average over a 10 min cycle) measured for clean and fouled membranes using either Instant Ocean (IO) or NaCl-based draw solutions.

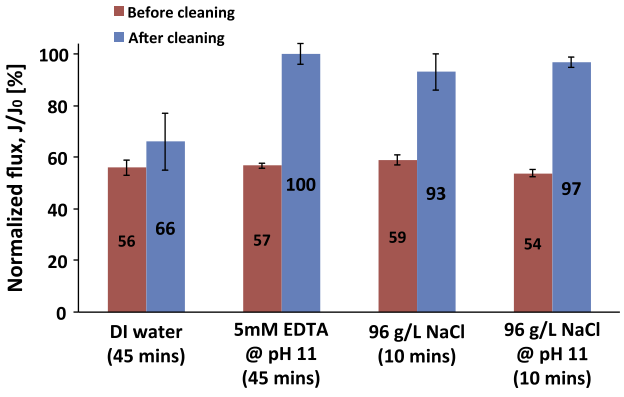

Fig. 6. Cleaning efficiency, defined as the ratio of the recovered flux to the initial RO flux, achieved using different cleaning methods, including pure physical cleaning with DI water, osmotic backwashing with and without NaOH addition, and chemical cleaning with a chelating agent at pH 11.

diminished despite the increased draw strength. Specifically, this may be due to the following mechanisms; first, as was already mentioned earlier, the long-time loss of permeation in this system is due to salt accumulation in the permeate space, which is expected to become greater for higher concentration draw solutions since it is diffusion-driven. Second, the initial flux decline is controlled by the dilutive concentration polarization in the feed channel, which, at constant mixing conditions, is dictated by the osmotic permeation rate. Both these mechanisms would also be present in the case of a clean membrane and are sufficient to explain why a higher draw solution becomes increasingly inefficient, as the flux does not vary linearly with driving force.

In the case of a fouled membrane this seems to be further exacerbated. The presence of a foulant layer deposited on the membrane surface could, in principle, affect both of these mechanisms contributing to loss of osmotic driving force. Fouled membranes generally exhibit reduced salt rejection in RO-mode, due to the lower water flux; this means that the initial permeate concentration would be higher (see Ramon et al. [12] for the effect of rejection on the osmotic flux decline); moreover, the foulant layer retards salt transport from the bulk feed channel to the membrane surface, thus increasing the dilution effect at the membrane surface (analogous to 'cake enhanced CP' [26]). In the case considered here, since the measured salt rejection of the fouled membranes was >99%, our previous results indicate that the effect of the initial permeate concentration is very weak; furthermore, the 'cake-enhanced dilution' at the membrane surface on the draw side would diminish the concentration driving force for salt diffusion. Hence, it is likely that, for the fouled membranes, the differences in observed flux decline between low and high-strength draw solution concentrations are caused by enhanced dilutive concentration polarization at the membrane surface.

4.2.2. Flux recovery with osmotic backwashing vs. chemical cleaning

Cleaning efficiencies obtained with either purely physical cleaning or with osmotic backwashing followed by physical cleaning are shown in Fig. 6. In general, flux decline during the accelerated 5-h fouling test reached ~60% of the initial RO flux (data showing the transient flux decline during the fouling tests is available in the supplementary material). This may be considered as an extreme case and is normally never reached in practice; the purpose here was to deliberately test these cleaning protocols under such extreme conditions, since successfully restoring flux for such heavily fouled membranes would suggest that a similar or better removal is possible for 'lighter' fouling (this assumption was tested during preliminary experimentation). Furthermore, it is possible that such a degree of fouling and flux decline may be present in localized regions or leading membrane elements, while the overall impact on the full system would remain much lower, on average.

Two important observations may be made based on our results. First, for the model system used in this study, physical cleaning is not an efficient method for restoring membrane performance; this has been observed previously (see, e.g., Jin et al. [19]). Second, cleaning efficiency is dependent on the solution chemistry, manifested here by the ionic composition of the draw solution. There appears to be a very weak correlation between the observed cleaning efficiency and the draw strength, that is, the osmotic permeation. Moreover, the cleaning efficiency obtained by the 32 g/L NaCl draw solution was greater than that achieved with a 64 g/L 'instant ocean' draw. This is an important observation as it points to the fact that the backwash effectiveness is not determined by a purely physical metric such as the osmotic permeation. This is discussed further in the following sections.

4.2.3. Effect of draw solution strength and composition

For the mono-valent, NaCl draw solutions, a weak trend of increased cleaning efficiency is observed for increased draw concentrations, which correspond with higher osmotic permeation rates. Increasing the backwash permeation rate corresponds with the purely physical component of the cleaning process. In a traditional backwash sense, this is expected to be a main determinant of cleaning efficiency. However, our results suggest that this need not be the case. Cleaning efficiencies using a seawater matrix at two different concentrations were low and, furthermore, only a very slight increase in efficiency was observed when the osmotic driving force was doubled. For both cases, the efficiency is substantially lower than that achieved with a pure NaCl draw solution of similar osmotic draw strength.

We believe the explanation to this is as follows. As already mentioned in the introduction, it is known that, in the presence of di-valent cations, the Alginate layer deposited at the membrane surface is denser, more cross-linked and may be strongly associated with the membrane surface through calcium bridging. These effects increase the fouling layer's impact on flux decline and render it more difficult to remove. It has been reported in the literature that a mono-valent salt solution may be used to clean an RO membrane fouled by Alginate, achieving 90% cleaning efficiency [18,22]. The proposed mechanism for this is that ion-exchange between the bulk and gel phases releases di-valent cations and weakens the mechanical integrity of the Alginate gel, rendering it more susceptible to physical removal. This mechanism is likely the reason for increased osmotic cleaning efficiency observed when NaCl-based

draw solutions were used. The efficiency obtained using the seawater-based draw, is believed to reflect a purely physical contribution of an additional perpendicular drag exerted by the permeation. For the case considered here, the purely physical effect of either crossflow-induced shear or the reversed permeation drag during a backwash cycle are found to be insufficient for any significant removal of the deposited layer. This result strongly suggests that for effective cleaning, a chemistry-based addition to the cleaning cycle, that might disrupt or weaken the inter-foulant interactions, is necessary.

4.2.4. Mechanisms of foulant removal

It is possible to trace three different contributions to the cleaning efficiency; one induced by fluid shearing, achieved by the physical cleaning; a combined shearing and lifting, achieved by backwashing with a seawater matrix; and a chemical interaction leading to structural weakening in conjunction with combined shearing/lifting, as achieved by the NaCl-based draw solution. The cleaning efficiency achieved by the NaCl-based draw is comparable with that obtained using a chemical cleaning solution, based on a chelating agent (di-sodium EDTA) in an elevated pH of 11, a proven recipe for efficient cleaning of organic fouling. Practically complete flux restoration was achieved when chemical cleaning was applied, as well as for the osmotic backwashing with 64 and 96 g/L NaCl-based draw, followed by physical cleaning with DI water.

We note that, when the highest strength draw was used (96 g/L NaCl), significant flux restoration was achieved immediately upon backwashing, without the additional DI-water physical cleaning. However, in this case, cleaning efficiency was not complete (95%), with only a slight improvement when the draw was at an elevated pH (97%) (Fig. 6). On the other hand, when lower draw strengths were used, flux restoration was only achieved upon further rinsing with DI water (Fig. 7).

The difference in the effectiveness of these protocols may be attributed to two possible explanations. Our data suggests that the cleaning is ultimately linked to the loosening of the gel matrix by ions exchanged between the bulk solution and gel phase; this mass exchange will depend on the driving force (concentration difference) and contact time. Since contact time is fixed in all experiments, a higher concentration will induce more rapid exchange of di-valent cations out of the gel matrix, weakening it and facilitating its physical removal from the membrane surface. In addition, a stronger draw is able to sustain a higher osmotic flux over the duration of the induced backwash cycle, which may be more effective in physically removing the weakened gel matrix; this could explain why a threshold may exist for an osmotic draw strength to become effective in removing the deposited foulant from the membrane surface. It is possible that for the lower strength draw solutions used in this study, contact time was sufficiently long to render the gel matrix susceptible to physical removal by the osmotic permeation. In these cases, shearing for a longer period (as achieved with the DI rinsing step) resulted in a substantial cleaning efficiency, the lowest being 92% for the 32 g/L NaCl draw.

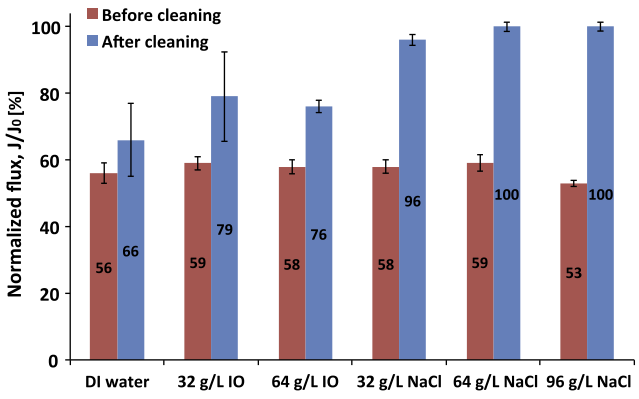

Fig. 7. Flux recovered (as % of the initial RO flux) by physical cleaning (recirculating DI water for 45 min) and osmotic backwashing using different draw solutions for 10 min, followed by physical cleaning. *Note*: IO – Instant Ocean.

These observations offer interesting and important insight into future optimization of osmosis-assisted cleaning protocols. For example, in some cases it may be possible to shorten the backwash duration substantially, through an appropriate coupling of a draw solution containing chemical agents that specifically target a foulant present; there may be a threshold draw-strength which will allow this relatively rapid cleaning to be achieved. In cases where exposure time to an appropriate chemical treatment is the key, rather than a physical removal mechanism, it may be beneficial to have a dual-stage process in which the first is a chemical rinse, then followed by an osmotic backwash step. Another possibility would be to have the osmotic capability of the draw approximately match the applied hydraulic pressure, effectively shutting down the permeation during a chemical rinse; in this case, the osmotic effect is not used as an additional physical removal mechanism, but as a means by which the chemical cleaning may proceed without the necessity of taking the cleaned modules off-line.

5. Conclusions

Osmotic backwashing, induced by replacing RO feed water with a highly concentrated salt solution, was evaluated in a lab-scale crossflow desalination simulator using commercial seawater RO membranes and a model organic foulant (alginic acid from brown algae) dispersed in an artificial seawater matrix. Numerical simulations have shown that relatively long pulse durations may be necessary in order to ensure that osmotic backwashing reverses permeation along the entire length of an RO system; for longer pulses, internal concentration polarization within the membrane support may be a limiting factor as it significantly reduces the reverse permeation rate. Experimental results indicate that osmotic backwashing can achieve similar flux recovery as conventional chemical cleaning methods. In the system studied, foulant removal was facilitated by the combined effect of chemical loosening of the Alginate gel and its subsequent removal by fluid shear; the loosening is achieved via the displacement of divalent cations by monovalent cations through a simple ion-exchange mechanism. Further experimentation may shed additional light on the relative role of these chemical and physical mechanisms. For example, draw strength optimization may be achieved by considering the contact time needed for effective ion exchange of divalent cations, while retaining sufficient osmotic draw power. Ultimately, it appears that the combination of the osmotically reversed permeation and a chemical composition, targeted at the foulant materials present, is the key to successful deployment of this method.

Acknowledgements

This research was supported in part by the UCLA Henry Samueli School of Engineering and Applied Science. Financial support for G.Z.R was provided by Vaadia-BARD Postdoctoral Fellowship Award Number FI-435-2010 through the United States–Israel Binational Agricultural Research and Development Fund. Financial support for T.V.N was provided by Vietnam National University-Hochiminh City.

Appendix A. Supplementary material

Supplementary data associated with this article can be found, in the online version, at http://dx.doi.org/10.1016/j.cej.2012.12.006.

References

[1] S. Wang, G. Guillen, E. Hoek, Direct observation of microbial adhesion to membranes, Environ. Sci. Technol. 39 (2005) 6461–6469.
[2] M. Raffin, E. Germain, S.J. Judd, Influence of backwashing, flux and temperature on microfiltration for wastewater reuse, Sep. Purif. Technol. 96 (2012) 147–153.
[3] T. Zsirai, P. Buzatu, P. Aerts, S. Judd, Efficacy of relaxation, backflushing, chemical cleaning and clogging removal for an immersed hollow fibre membrane bioreactor, Water Res. 46 (14) (2012) 4499–4507.
[4] C. Fritzmann, J. Lowenberg, T. Wintgens, T. Melin, State-of-the-art of reverse osmosis desalination, Desalination 216 (2007) 1–76.
[5] A. Sagiv, R. Semiat, Backwash of RO spiral wound membranes, Desalination 179 (1–3) (2005) 1–9.
[6] J. Qin, M. Oo, K. Kekre, H. Seah, Preliminary study on novel backwash cleaning for reverse osmosis fouling control in water reuse, Water Sci. Technol. 10 (3) (2010) 296–301.
[7] J. Qin, M. Oo, K. Kekre, H. Seah, Optimization of direct-osmosis-high-salinity cleaning for reverse osmosis fouling control in water reuse, Water Sci. Technol. 10 (5) (2010) 800–805.
[8] J. Qin, H. Oo, K. Kekre, B. Liberman, Development of novel backwash cleaning technique for reverse osmosis in reclamation of secondary effluent, J. Membr. Sci. 346 (2010) 8–14.
[9] K.S. Spiegler, J.H. Macleish, Molecular (osmotic and electro-osmotic) backwash of cellulose acetate hyperfiltration membranes, J. Membr. Sci. 8 (2) (1981) 173–192.
[10] Y. Liberman, RO membrane cleaning method. US patent 76588852B2.
[11] A. Sagiv, N. Avraham, C.G. Dosoretz, R. Semiat, Osmotic backwash mechanism of reverse osmosis membranes, J. Membr. Sci. 322 (1) (2008) 225–233.
[12] G. Ramon, Y. Agnon, C. Dosoretz, Dynamics of an osmotic backwash cycle, J. Membr. Sci. 364 (1–2) (2010) 157–166.
[13] A. Sagiv, R. Semiat, Modeling of backwash cleaning methods for RO membranes, Desalination 261 (3) (2010) 338–346.
[14] S. Li, S. Heijman, J. Verberk, A. Verliefde, A. Kemperman, J. van Dijk, G. Amy, Impact of backwash water composition on ultrafiltration fouling control, J. Membr. Sci. 344 (1–2) (2009) 17–25.
[15] S. Li, S. Heijman, J. Verberk, P. Le Clech, J. Lu, A. Kemperman, G. Amy, J. van Dijk, Fouling control mechanisms of demineralized water backwash: reduction of charge screening and calcium bridging effects, Water Res. 45 (19) (2011) 6289–6300.
[16] S. Hong, M. Elimelech, Chemical and physical aspects of natural organic matter (NOM) fouling of nanofiltration membranes, J. Membr. Sci. 132 (1997) 159–181.
[17] W. Ang, S. Lee, M. Elimelech, Chemical and physical aspects of cleaning of organic-fouled reverse osmosis membranes, J. Membr. Sci. 272 (1–2) (2006) 198–210.
[18] S. Lee, M. Elimelech, Salt cleaning of organic-fouled reverse osmosis membranes, Water Res. 41 (5) (2007) 1134–1142.
[19] X. Jin, X. Huang, E. Hoek, Role of specific ion interactions in seawater RO membrane fouling by alginic acid, Environ. Sci. Technol. 43 (10) (2009) 3580–3587.
[20] A. Subramani, E. Hoek, Biofilm formation, cleaning, re-formation on polyamide composite membranes, Desalination 257 (1–3) (2010) 73–79.
[21] S. Madaeni, S. Samieirad, Chemical cleaning of reverse osmosis membrane fouled by wastewater, Desalination 257 (2010) 80–86.
[22] W. Ang, A. Tiraferri, K. Chen, M. Elimelech, Fouling and cleaning of RO membranes fouled by mixtures of organic foulants simulating wastewater effluent, J. Membr. Sci. 376 (1-2) (2011) 196–206.
[23] W. Ang, N. Yip, A. Tiraferri, M. Elimelech, Chemical cleaning of RO membranes fouled by wastewater effluent: achieving higher efficiency with dual-step cleaning, J. Membr. Sci. 382 (2011) 100–106.
[24] T. Cath, A. Childress, M. Elimelech, Forward osmosis: principles, applications, and recent developments, J. Membr. Sci. 281 (2006) 70–87.
[25] N.Y. Yip, A. Tiraferri, W.A. Phillip, J.D. Schiffman, M. Elimelech, High performance thin-film composite forward osmosis membrane, Environ. Sci. Technol. 44 (2010) 3812–3818.
[26] E.M.V. Hoek, M. Elimelech, Cake-enhanced concentration polarization: a new fouling mechanism for salt-rejecting membranes, Environ. Sci. Technol. 37 (24) (2003) 5581–5588.